Adsorption and reactions of CH_2I_2 on clean and oxygen-modified Ag(111): a RAIRS and TPD study

K.C. Scheer[a], A. Kis[b], J. Kiss[b] and J.M. White[a,*]

[a] *Center for Materials Chemistry, Department of Chemistry and Biochemistry, University of Texas at Austin, Austin, TX 78712, USA*
E-mail: jmwhite@mail.utexas.edu

[b] *Reaction Kinetics Research Group of Hungarian Academy of Sciences, University of Szeged, Szeged, Hungary*

The surface chemistry of CH_2I_2 on Ag(111) in the presence and absence of pre-adsorbed O, produced by NO_2 adsorption at elevated temperature, has been examined using temperature-programmed desorption and reflection absorption infrared spectroscopy. There is good evidence for the formation of adsorbed methylene, CH_2(a), that reacts with another CH_2(a) to form and desorb ethylene, C_2H_4(g), in a reaction-limited process. Increasing the surface coverage of CH_2I_2 hinders both the dissociation and recombination processes indicated by the upward temperature shift in the formation of C_2H_4. Co-adsorbed O atoms strengthen the bonding of CH_2I_2 to the surface; the increased thermal stability is up to 60 K. The formation of C_2H_4 decreases with increasing amounts of pre-adsorbed O; the main reaction product is CH_2O produced in a reaction-limited process. CH_2O forms either on the chemisorbed or on the oxide phase with desorption peak temperatures of 225 and 270 K, respectively. The formation of gas-phase carbon dioxide suggests that a formate intermediate is involved in a secondary reaction pathway.

KEY WORDS: CH_2I_2 surface chemistry; CH_2I_2 on silver; oxygen-modified silver

1. Introduction

Studies of the reaction of hydrocarbon fragments (C_xH_y) on metal surfaces are a key component in understanding the mechanism of the Fisher–Tropsch synthesis and the transformation of methane to other hydrocarbons [1,2]. Previous studies indicate that Ag(111) is a unique surface on which C_xH_y fragments undergo exclusively recombination to form higher hydrocarbons even under ultrahigh vacuum (UHV) conditions [3–5]. This unique property of Ag(111) contrasts with most transition metal surfaces on which decomposition of C_xH_y fragments dominates [6] and is consistent with the high-pressure catalytic properties of silver [7]. Studies of the adsorption and thermal-, UV photon-, or electron-induced decomposition of alkyl halides on single-crystal surfaces provide a good understanding of how to prepare alkyl species on metal surfaces [6,8].

A further aspect of this research is to examine the reaction of hydrocarbon fragments with pre-adsorbed oxygen to produce oxygenated surface complexes, which are reaction intermediates in catalytic synthesis of alcohols and aldehydes. CH_2 surface species partially oxidize to formaldehyde on Pt(111) [9], Pd(100) [10], Rh(111) [11–13], Cu(100) [14], and Ru(001) [15]. These studies suggest that direct addition of transient methylene to surface oxygen leads to formaldehyde production.

As catalytic epoxidation of ethylene over silver is an industrially important reaction, studying the reactivity of Ag(111) pre-covered with O has particular significance [16]. The formation of different O phases on Ag(111) has been studied in detail, focusing on the analysis of O species accommodating interstitial, overlayer, or bulk sites [17,18] and the surface morphology of the O-covered surface [19–21]. The reaction between O and hydrocarbon species adsorbed on Ag(111), however, has not been investigated up to this point.

In the present work we report on the adsorption and dissociation of CH_2I_2 on clean and O-modified Ag(111). The methods used are temperature-programmed desorption (TPD) and reflection absorption infrared spectroscopy (RAIRS). On clean Ag(111), at 80 K, low-exposure CH_2I_2 dissociates to form adsorbed methylene, CH_2(a), which recombines and desorbs as ethylene at various temperatures. As the dose increases, formation of CH_2(a) is shifted to higher temperature due to crowding on the surface. O(a) acts not only as a site blocker, limiting the decomposition of CH_2I_2, but also as a reaction partner to form formaldehyde in a reaction-limited process. A secondary reaction in which CH_2I_2 reacts directly with O(a) to form formate is also proposed.

2. Experimental

Experiments were performed in a two-level UHV chamber with a base pressure of $4\ 10^{-10}$ torr. The lower chamber was equipped with standard surface analysis tools including a single-pass cylindrical mirror analyzer (Physical Electronics) for Auger electron spectroscopy (AES) and a differentially pumped quadrupole mass

*To whom correspondence should be addressed.

1022-5528/02/0700-0043/0

spectrometer (Extrel C-50) for TPD measurements. The TPD spectra were recorded at a heating rate of 2 K/s and the quadrupole was multiplexed such that 11 masses could be recorded simultaneously.

The upper level of the UHV system consisted of a 4 in. inner diameter cylindrical chamber, which was coupled to a commercial Fourier transform infrared spectrometer (Nicolet, Magna IR 860) for RAIRS experiments. The infrared beam entered and exited the chamber through differentially pumped O-ring sealed KBr windows and was focused at a grazing angle of 82° with respect to the surface normal of the 13 mm diameter Ag(111) substrate. The exiting beam was p-polarized with a ZnSe wire grid polarizer before being focused onto a narrow-band HgCdTe (MCT) detector with a single 82° off-axis ellipsoidal mirror. Infrared spectra were recorded by adding 1500 scans at 4 cm^{-1} resolution. The sample background for each absorbance spectrum was taken from either I-covered Ag(111), produced by annealing the sample to 350 K to desorb all hydrocarbon fragments, or O-pre-covered Ag(111) prior to CH_2I_2 exposure. The upper chamber also housed a residual gas analyzer (Stanford Research Systems, SRS-RGA).

The sample holder, constructed in-house, allowed the Ag(111) substrate (Monocrystal Co., 99.995%) to be resistively heated to 975 K and liquid nitrogen cooled to 77 K. The sample temperature was measured using a chromel–alumel-type thermocouple that was inserted into a small hole on one edge of the crystal. The substrate surface was cleaned by repeated cycles of Ar^+ grazing-incidence sputtering at 300 K (2.5 kV, 10 min) and annealing (750 K, 3 min). This cleaning procedure was repeated until impurity concentrations were below the detection limit of AES.

The adsorbate, methylene iodide (CH_2I_2, Lancaster, 99%), was purified by several freeze–pump–thaw cycles prior to each experiment. No impurities were identified by mass analysis. Each dose involved placing 0.11 mbar of gas, measured with a Baratron gauge, behind a preset open leak valve connected to a cylindrical tube (3 mm internal diameter, 60 mm in length) that terminated 3 cm in front of the Ag(111) surface. With the sample holder and substrate at cryogenic temperatures, the chamber pressure rose to $\sim 10^{-9}$ torr during exposure. The dose was initiated when a butterfly valve allowed the gas to flow through the leak valve to the substrate and was terminated after a designated time for the desired surface coverage (1–20 min) by pumping the residual gas in the gas line with a turbomolecular pump. Exposure is reported in terms of "standard dose" (SD) units. One SD CH_2I_2 is defined as the highest exposure that does not exhibit a multilayer peak in TPD.

As the dissociation probability of molecular oxygen on Ag(111) is very low, except at high pressure and temperature [19,22], Ag(111) pre-covered with oxygen was prepared by NO_2 adsorption [23–25] at elevated temperature. NO_2 was dosed from a quartz capillary tube positioned along the surface normal. The chemical reaction for adsorption is

$$NO_2(g) \rightarrow NO(a) + O(a) \quad (1)$$

During exposure, the sample temperature was held at 515 K to desorb NO(a). This temperature is low enough to prevent combination of O(a):

$$2O(a) \rightarrow O_2(g) \quad (2)$$

The dose was initiated by allowing $NO_2(g)$ into the gas line through a Nupro valve. The pressure in the gas line remained constant during the exposure, at some pressure indicated by the desired coverage (10–250 mtorr measured by a thermocouple gauge in the gas line). The pressure rise in the chamber was of the order of 10^{-7}–10^{-8} torr. After the appropriate amount of time had elapsed for the desired surface coverage (1–5 min), the pressure of $NO_2(g)$ was removed from the gas line with a turbomolecular pump, consequently ending the exposure. O(a) coverage is reported in terms of ML, where 0.5 ML of O is defined as the saturated p(4 × 4) O-covered Ag(111) surface [19,26]. Following adsorption, the crystal was cooled to 80 K, during which time TPD and RAIRS indicated that no detectable re-adsorption of gas-phase NO_2 had occurred.

The adsorbed oxygen was detectable by a distinct TPD feature at ~570 K. The peak area as a function of exposure shows Langmuir-type behavior with two distinct saturation curves. The two different regimes are clearly visible and agree with the literature on O adsorption on Ag(111) [19,23,26], which indicates that the decomposition of NO_2 produced overlayers having the same structure as those produced using oxygen at high pressures. Bare *et al.* [23] reported that producing atomic oxygen overlayers by NO_2 decomposition at 500–520 K results in an absolute coverage of (4 × 4)O–Ag(111) of 7.07 (±0.55) 10^{14} O atoms/cm^2, or 0.51 ± 0.04 ML. First, the chemisorbed layer is formed (0.14 ML) and on top of it a single trilayer structure of Ag_2O is produced. The superstructure gives a coincidence p(4 × 4) mesh relative to the underlying Ag(111) substrate in LEED. In our experiments, the rough exposure vs. coverage function shows its first saturation just below 0.2 ML. The 0.1 ML O coverage experiments denote this first saturation state.

3. Results

3.1. CH_2I_2 on clean Ag(111)

3.1.1. TPD results

Figure 1(A) shows the desorption of CH_2I_2 from clean Ag(111) following adsorption of CH_2I_2 at 78 K. These spectra follow the desorption of 127 amu, which tracks both parent and iodine desorption from the surface. The small desorption feature at low exposure that

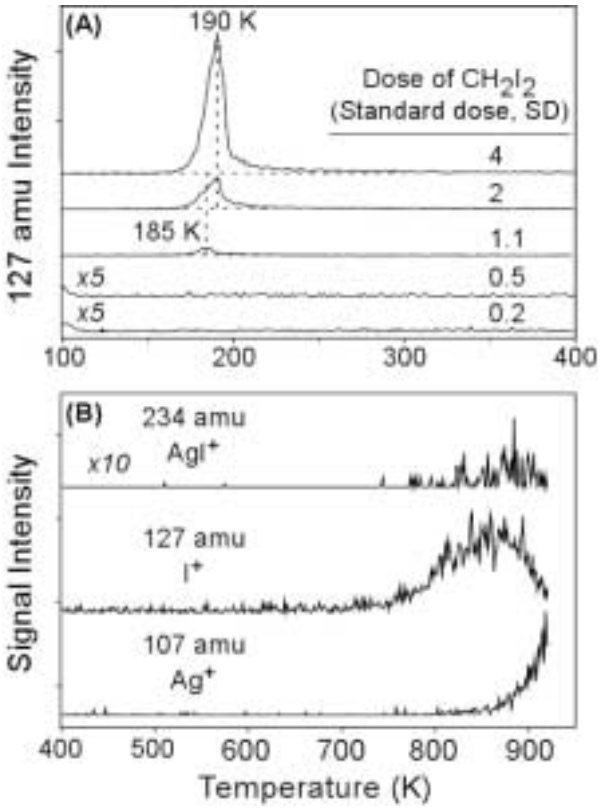

Figure 1. (A) Desorption of CH_2I_2, following I^+ signal of 127 amu, from clean Ag(111) following adsorption of varying exposures of CH_2I_2 at 78 K. (B) Time-of-flight TPD signals of the given mass numbers following adsorption of 2 SD CH_2I_2 at 78 K.

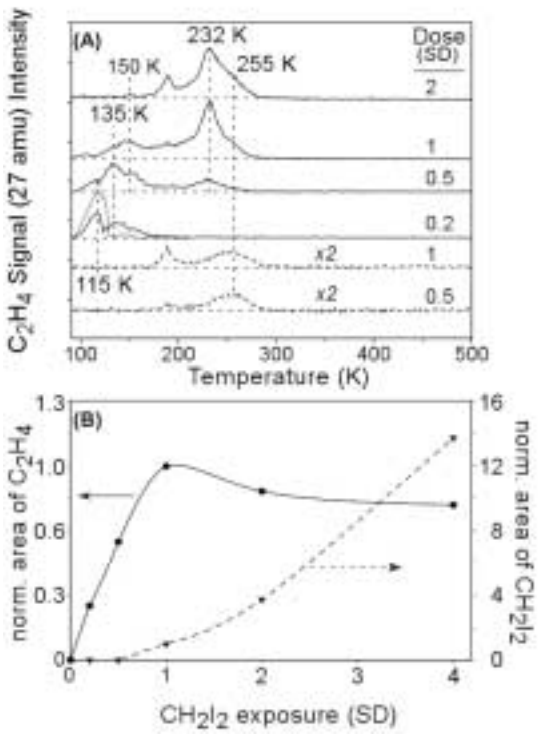

Figure 2. (A) C_2H_4 desorption from clean Ag(111) after adsorption of varying exposures of CH_2I_2 at 78 K. The dashed curves correspond to (0.2 SD) C_2H_4 desorption after adsorption of C_2H_4 at 78 K and (0.5–1 SD) C_2H_4 desorption after adsorption of CH_2I_2 at 78 K on Ag(111) pre-saturated with I. (B) Normalized integrated peak areas from the desorption of C_2H_4 (27 amu) and CH_2I_2 (127 amu) from clean Ag(111) vs. initial dose of CH_2I_2. The signals were normalized with respect to the integrated peak area of the features from 1 SD CH_2I_2 on clean Ag(111).

appears at ~100 K is attributed to irreproducible desorption from non-sample surfaces and is ignored in subsequent analysis. At low exposure, 0.2 and 0.5 SD, there is no detectable parent desorption, indicating that the parent dissociates either upon adsorption of the molecule or during the temperature ramp of the experiment. At 1.1 SD exposure, a desorption feature appears at 185 K that grows with increasing exposure and shifts to 190 K at 4 SD exposure. The desorption temperature shifts to higher temperature with increasing surface coverage indicating that desorption occurs from the condensed layer.

Figure 1(B) shows TPD features at high mass and high temperature following a 2 SD exposure at 78 K done in a separate chamber equipped for time-of-flight mass spectrometry. Iodine (127 amu) desorbs in a broad feature that spans from 750 K to temperatures greater than 900 K. AgI^+ (234 amu) and Ag^+ (107 amu) were also detected in low concentrations at temperatures above 800 K, but other products such as I_2 and Ag_xI_y clusters, if they desorb, were not detectable.

The only other desorption product from CH_2I_2 adsorbed on clean Ag(111) is C_2H_4. The solid lines of figure 2(A) show the TPD curves for 27 amu as a function of CH_2I_2 exposure on clean Ag(111). All 27 amu signals in figure 2(A) are ascribed to ethylene, except the small peak at 185 K after 2 SD exposure, which, on the basis of fragmentation pattern analysis, is assigned to the parent molecule, CH_2I_2. The figure also shows the effect of pre-adsorbed I on the formation of C_2H_4 from 0.5 and 1 SD of CH_2I_2 (dashed curves $\times 2$ intensity). Pre-adsorbed I was produced by adsorption of CH_2I_2 at 78 K followed by annealing above 500 K, a temperature at which all hydrocarbon fragments desorb leaving only I(a). Finally, an I-saturated surface was dosed with 0.2 SD of C_2H_4 and shows a peak at 115 K (dashed curve superimposed on the solid curve corresponding to 0.2 SD exposure of CH_2I_2 on clean Ag).

There are interesting dose-dependent changes in these spectra. On clean Ag(111), after 0.2 SD CH_2I_2 exposure, C_2H_4 desorption exhibits peaks at 115 and 135 K. As the initial exposure increases to 0.5 SD, the 115 K peak decays, the 135 K peak increases, intensity in the 150 K region increases, and a peak at 232 K emerges. Increasing the exposure to 1 and 2 SD causes the C_2H_4

desorption temperature to shift to even higher temperatures with reduced contributions from low-temperature peaks. At 1 SD, the 135 K peak is suppressed, the 150 K region intensifies and there is strong growth of the 232 K peak with an obvious high-temperature shoulder extending to 275 K. At 2 SD, the spectrum is dominated by the 232 K peak, there is emergence of molecular desorption of CH_2I_2 at 185 K, and there is negligible intensity below 175 K. In the presence of saturation pre-adsorbed I(a), the C_2H_4 desorption feature decreases in intensity (the peak area is 16–20% of the peak area of the same dose from the clean surface), the low-temperature peaks disappear, and the peak temperature shifts to 255 K.

The integrated TPD peak areas of CH_2I_2 and C_2H_4 as a function of initial dose of CH_2I_2 are shown in figure 2(B). The integrated peak area of 1 SD CH_2I_2 adsorbed on clean Ag(111) is used as a reference for normalization of all the peak areas shown on the graph. The integrated peak area of the 27 amu curve is due exclusively to C_2H_4 as the contribution of CH_2I_2 to this mass was subtracted from the total integrated area. The amount of the total desorbed C_2H_4 reaches a maximum at 1 SD, above which it shows a slight decrease in intensity. At the same dose, CH_2I_2 appears as a desorption product and its magnitude increases dramatically with increasing coverage.

3.1.2. RAIRS results

Figure 3 shows the RAIR spectra of 0.2 and 2 SD CH_2I_2 adsorbed at 78 K. Also shown are spectra of 2 ML CH_2I_2 annealed to various temperatures and then cooled before scanning at 80 K. When 0.2 SD CH_2I_2 was adsorbed on clean Ag(111) at 78 K, four features are present in the infrared spectrum at 2910, 1345, 1110, and 820 cm^{-1}. As the coverage increases to 2 SD, the 1110 cm^{-1} feature increases in intensity, features appear at 3044 and 2968 cm^{-1}, and the 2910 cm^{-1} feature shifts to 2902 cm^{-1}. When 2 SD CH_2I_2 is annealed to 140 K, the intensities of the features at 1345, 1110, and 820 cm^{-1} increase. Annealing to 170 K causes a decrease in the intensity of the feature at 3044 cm^{-1}, and after annealing to 200 K only bands at 2910, 2902, and 2845 cm^{-1} are visible. At 220 K, the 2902 cm^{-1} peak is still present as a shoulder of the 2910 cm^{-1} peak. At 240 K, these features are indistinguishable from the noise level of the detector.

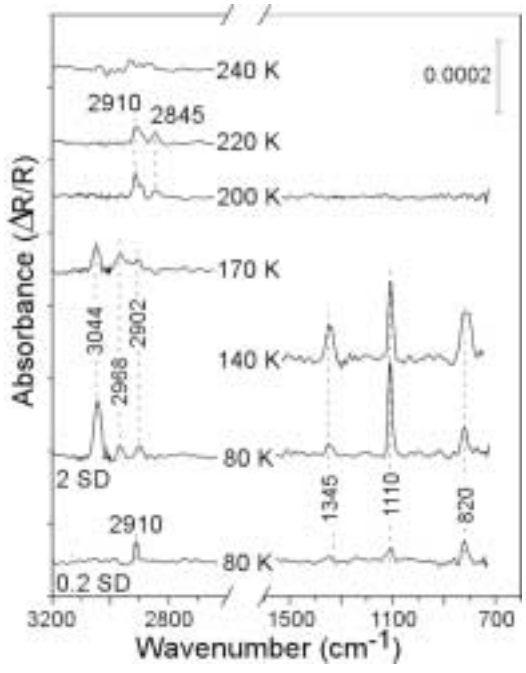

Figure 3. RAIR spectra of 0.2 and 2 SD CH_2I_2 adsorbed at 80 K and after annealing to elevated temperatures following adsorption of 2 SD CH_2I_2 on clean Ag(111) at 80 K. All spectra were obtained at 80 K.

3.2. CH_2I_2 on Ag(111) pre-covered with O

3.2.1. TPD results

When CH_2I_2 is dosed onto Ag(111) in the presence of pre-adsorbed O, new TPD products appear. Figure 4 shows the TPD spectra for 1 SD CH_2I_2 adsorbed on Ag(111) predosed with O. The O coverage was varied from 0 to 0.5 ML, where 0.5 ML is the saturation coverage of O on Ag(111). Two masses are shown in figure 4: 30 amu, following the desorption of CH_2O, is shown by the solid lines and 44 amu, following CO_2 desorption, is represented by the inserted lines. When 1 SD CH_2I_2 was adsorbed on clean Ag(111), as expected no CH_2O or CO_2 desorption was observed. The small 30 amu feature at 185 K is attributable to the desorption of parent

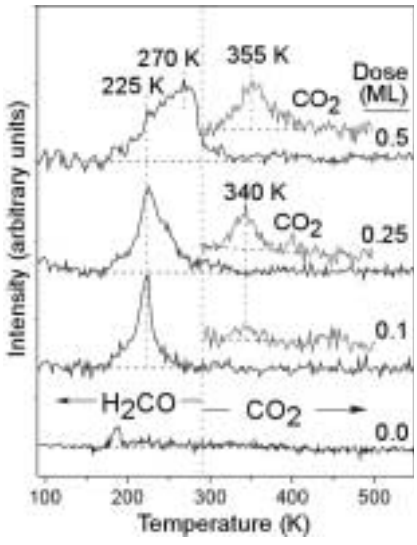

Figure 4. Desorption of CH_2O (30 amu; solid line) and CO_2 (44 amu; dotted line) following adsorption of 1 SD CH_2I_2 at 80 K on Ag(111) pre-adsorbed with varying amounts of O(a). The intensity of the spectra corresponding to CO_2 desorption has been multiplied by four.

CH_2I_2. When 0.1 ML O is pre-adsorbed before CH_2I_2 adsorption, a large feature at 225 K emerges indicative of CH_2O desorption. At this coverage, there is also a faint, but reproducible, CO_2 desorption signal at 340 K. As the O coverage is increased to 0.25 ML, the CH_2O desorption feature becomes asymmetric forming a high-temperature shoulder and the CO_2 peak at 340 K intensifies. Finally, when saturation oxygen coverage is reached, the CH_2O peak changes shape dramatically: the peak becomes asymmetric, the maximum intensity is now at 270 K, the peak has a significant low-temperature component at 225 K, and the intensity drops sharply to the baseline at ~280 K. Also, the CO_2 feature intensifies and shifts to 355 K.

The effect of pre-adsorbed oxygen (0.1, 0.25, and 0.5 ML) on the other major desorption product, C_2H_4, from 0.5 SD CH_2I_2 at 80 K is shown in figure 5. For comparison purposes, the desorption of C_2H_4 after dosing CH_2I_2 on 0.33 ML I(a) and clean Ag(111) are also shown. Compared to the clean surface, when 0.1 ML O is pre-adsorbed, the lower temperature C_2H_4 desorption peak shifts to higher temperature, ~170 K, and the intensities of both the low- and high-temperature features decrease by approximately 30%. When the coverage of pre-adsorbed O increases to 0.25 ML, the lower-temperature feature disappears and the intensity of the 230 K peak decreases further until finally, when 0.5 ML of O is pre-adsorbed, the saturation coverage of O, no ethylene desorption is detectable. At this coverage of O, no ethylene desorption is observable at any CH_2I_2 exposure (not shown).

3.2.2. RAIRS results

Figure 6 shows the RAIR spectra of 0.5 SD CH_2I_2 adsorbed on O-saturated Ag(111) as a function of annealing temperature. After annealing, the sample was allowed to cool to 80 K before the spectra were collected. At 80 K, three features are observed at 3057, 2974, and 1114 cm^{-1}. Annealing to 200 K causes the intensity of these features to decrease and the vibrations in the CH stretching region to blue shift slightly to 3060 and 2979 cm^{-1}, respectively. After annealing to 220 K, three features are still observable; their intensity has again decreased. After annealing to 260 K, of the three original features only the 3060 cm^{-1} peak remains and again the intensity decreases. There is also a very weak reproducible vibration at 2810 cm^{-1}. After annealing to 350 K, no vibrations are observable.

4. Discussion

4.1. Thermally activated reactions of CH_2I_2 on clean Ag(111)

When dosed on clean Ag(111), the results are interpreted in terms of non-dissociative adsorption of CH_2I_2 at 78 K, dose-dependent C–I bond breaking during the early stages of TPD, and methylene recombination and desorption at various stages. This model is consistent with the information shown in figure 1(A), which indicates the lack of parent desorption below 1 SD CH_2I_2. More revealing, however, are the C_2H_4 TPD results. The

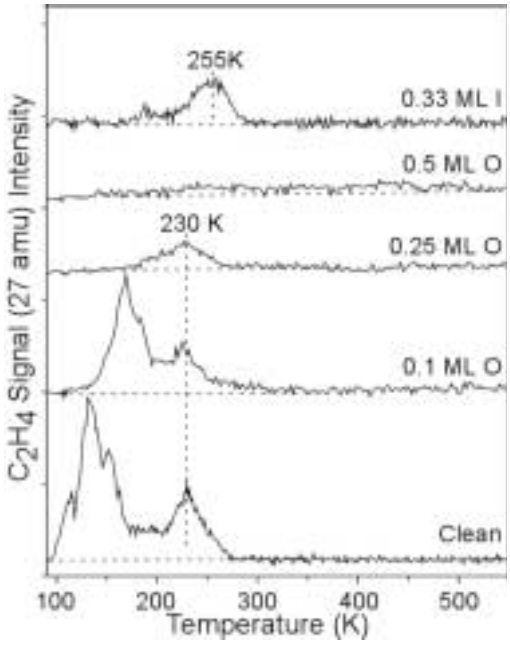

Figure 5. Formation of C_2H_4 on I- and O-modified Ag(111). CH_2I_2 adsorption on the clean surface is shown for reference. In each case 0.5 SD CH_2I_2 was dosed at 78 K.

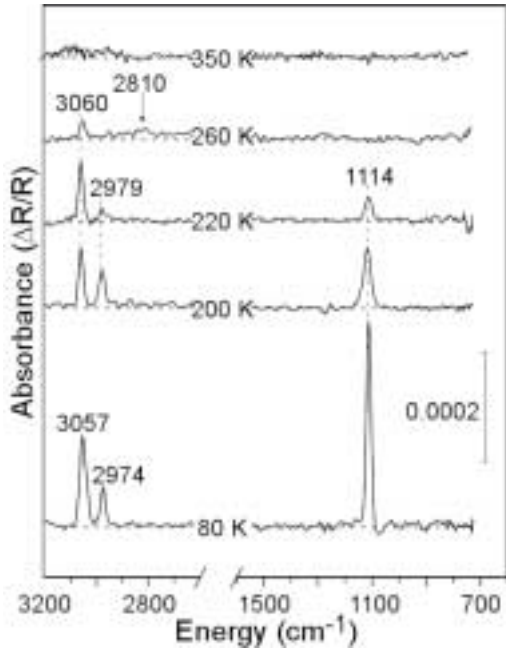

Figure 6. RAIR spectra of 0.5 SD CH_2I_2 at 80 K and annealed to higher temperatures adsorbed on Ag(111) surface saturated with O.

dashed 0.2 SD CH_2I_2 curve in figure 2(A) denotes that C_2H_4 dosed directly onto Ag(111) pre-covered with I desorbs at 115 K. C_2H_4 desorption at 115 K occurs at low exposure after 0.2 and 0.5 SD CH_2I_2, but not for higher exposures. Thus, there is evidence for C–I bond cleavage at temperatures less than 115 K provided that the dose is small and there are many sites to accommodate the decomposition products, 2I(a) and CH_2(a). Upon increasing the dose from 0.2 to 0.5 SD, the total integrated TPD peak area for C_2H_4 increases by a factor of approximately 2 and the intensity shifts to being dominated by reaction-limited processes. Doubling the dose again, to 1 SD, maxima are present below and above the CH_2I_2 parent desorption temperature (185 K) and the C_2H_4 normalized integrated intensity is chosen to be 1.00 as a reference. Doubling the dose to 2 SD, the total integrated C_2H_4 intensity decreases slightly to 0.87 and there is increased CH_2I_2 desorption, as shown in figure 2(B).

These desorption intensity shifts are attributed increased site blocking and less parent dissociation at low temperatures as the initial CH_2I_2 dose increases. In other words, on a surface crowded with CH_2I_2, sites for incorporating three fragments, 2I(a) and CH_2(a), are not available until the thermal energy is high enough to displace surrounding CH_2I_2 by desorption. CH_2I_2 in the multilayer accounts for the 27 amu peak at 185 K after 2 SD CH_2I_2 exposure. Above this temperature, at this exposure the surface is saturated with a mixture of I(a) and CH_2(a). There is negligible C_2H_4 desorption below 200 K because there is not significant C–I bond cleavage until CH_2I_2 begins to desorb at approximately 175 K. For lower exposures, similar site blocking effects on C–I bond breaking also apply, but the activation energy requirements to supply sufficient adsorption sites for 2 I(a) and CH_2(a) are met at lower temperatures.

To study the effect of site blocking on the desorption of ethylene, a surface with 0.33 ML I(a) (slightly less than saturation) was prepared. Figure 2(A) compares the ethylene desorption signal from clean (solid trace) and Ag(111) pre-covered with I (dashed 0.5 and 1 SD trace) after CH_2I_2 adsorption. Pre-adsorbed I caused the C_2H_4 desorption feature to decrease in intensity and to shift from 230 to 255 K, indicating that I(a) hinders the coupling of CH_2(a) groups. The effects of site blocking are obvious. First, a significant drop in the ethylene desorption is observed as the TPD peak area from the I-pre-covered surface is only 15% of that from the clean substrate for 1 SD CH_2I_2 exposure. The second effect is the dramatic increase of the parent desorption when I(a) is present (not shown), the peak area is 4.57 times larger than the peak area from the clean surface for 1 SD CH_2I_2 exposure. Also, the C_2H_4 desorption feature has shifted into the region above the molecular CH_2I_2 desorption temperature (185 K). Evidently, C_2H_4 desorption arises from the recombination of CH_2(a) groups that are formed by C–I bond breaking at or below 185 K and are stabilized by the presence of large quantities of I(a). Pre-adsorbed I is also responsible for the emergence of high-temperature tailing of the C_2H_4 desorption features from clean Ag(111). Adsorbed I is produced in the decomposition reaction of the parent CH_2I_2 molecules, but the distribution of I(a) is not as homogeneous on the surface as in the pre-covered case, which is apparent by the large TPD peak intensity at 232 K from the "clean" surface, i.e. areas with no I(a) present.

The RAIR spectra presented in figure 3 indicate that CH_2I_2 adsorbs dissociatively on Ag(111) at low exposures (0.2 SD) and adsorbs intact at higher exposures (2 SD). The peaks characteristic of adsorbed CH_2I_2 (3045, 2968, 1345, 1110, and 820 cm^{-1}) disappear when the sample is annealed to 200 K in agreement with TPD results that indicate that the parent desorbs at 185 K. The only species present on the surface above this temperature are CH_2(a) and I(a). Between 80 and 170 K, except for the 1345 and 820 cm^{-1} features, the intensity of the peaks assigned to CH_2I_2 continuously decrease with annealing indicating that the dissociation of the parent is below the onset of parent desorption. In this temperature regime, the bands at 820 and 1345 cm^{-1} significantly intensify and the peak at 2902 cm^{-1} does not change in either intensity or position. The changes in intensity of vibrational modes characteristic of CH_2I_2 with temperature indicate the presence of dipole–dipole interactions and/or thermally induced modification of the adsorption geometry of CH_2I_2 on Ag(111).

CH_2I_2 is known to crystallize into different phases depending on the final temperature of the solid and the process of cooling [27]. CH_2I_2 has two stable phases: above 258 K there is a stable phase, phase I, that transforms reversibly into a second stable phase, phase II, during slow cooling. Rapid cooling below 200 K causes the metastable phase I' to form directly. On warming, this metastable phase I' transforms to phase II near 200 K. Phase I' is a monoclinic-like structure.

In the current experiments, CH_2I_2 was dosed onto Ag(111) at 78 K. This procedure corresponds to rapid cooling, and condensed CH_2I_2(a) would correspond to phase I'. The vibration assignments of CH_2I_2 in our experiment are compared to those reported in the literature in table 1. CH_2I_2/Ag(111) stretching modes were observed at 3044 and 2968 cm^{-1}, which indicate that either the adsorbate has condensed in a disordered liquid-like phase or distortion of the crystal structure has occurred [28]. The latter explanation is inadequate, however, because 2 SD does not form a thick multilayer necessary to form a real crystal structure. Thus, the metastable phase I' does not form on the Ag(111) surface in spite of the rapid cooling, but the adsorbed CH_2I_2 molecules are mobile. This model of adsorbate mobility is in agreement with the behavior of other halohydrocarbons adsorbed on single-crystal surfaces [29].

Table 1
CH_2I_2 vibrational assignments (cm^{-1}).

	CH_2I_2(l) [38]	CH_2I_2(s) phase I' [27]	CH_2I_2/Mo(110) [30]	CH_2I_2/Rh(111) [11]	CH_2I_2/Ag(111)
ν_a(MCM)	484	485			
δ(MCM)	570	573	570		
$\rho(CH_2)$	716	717.5–719	750	720	820
$\gamma(CH_2)$	1031		1030	1080	
$\omega(CH_2)$	1105	1095–1100	1100		1110
$\delta(CH_2)$	1350	1345	1390	1350	1345
$\nu_s(CH_2)$	2967	2959	2960	2940	2968
$\nu_a(CH_2)$	3047	3041	3060	3030	3044

In the case of CH_2I_2 adsorbed on Ag(111), the CH_2 rocking mode at 820 cm^{-1} is blue shifted significantly from the liquid- and solid-phase frequencies of 716 and 729 cm^{-1}, respectively. This mode cannot be assigned to adsorbed CH_2 because it disappears, along with the other vibrational modes of CH_2I_2, after annealing to 200 K. The vibrational frequency of the CH_2 rocking mode of CH_2I_2 adsorbed on an Mo(110) surface also shows a significant blue shift compared to liquid- and solid-phase CH_2I_2 [30].

When CH_2I_2 was adsorbed on Al(111) at 98 K, Kondo *et al.* [28] observed two features that were attributed to CH_x: most likely CH_2 groups on the surface at 2918 and 2848 cm^{-1}. The peak positions and intensities were not sensitive to coverage or temperature up to multilayer doses and 193 K. On Rh(111), RAIRS data showed two bands at 2937 and 2863 cm^{-1} characteristic of CH_2 species [31]. In our study of CH_2I_2 on Ag(111), interestingly, the peak that is assigned to the asymmetric CH_2 stretching mode in CH_2(a) is perturbed by the presence of CH_2I_2(a) and I(a), the frequency ranging from 2902 to 2910 cm^{-1}. After 0.2 SD CH_2I_2 exposure, there is a peak at 2910 cm^{-1}. For 2 SD CH_2I_2 exposure, the frequency is at 2902 cm^{-1}. After annealing the 2 SD CH_2I_2 exposure to 200 K, there are three distinct peaks at 2902, 2910, and 2845 cm^{-1}, and after annealing to 220 K, there is an asymmetric peak at 2910 cm^{-1} that has a 2902 cm^{-1} component and there is no change in the 2845 cm^{-1} feature. The bands at 2910 and 2845 cm^{-1} are assigned to CH_2(a) on Ag(111) and the band at 2902 cm^{-1} is assigned to the CH_2(a) vibration softened by the presence of I(a).

Above 200 K, the only vibrational bands visible are seen in the stretching region. Normally the deformation bands of C_xH_y species are more intense [13,32]. Fan and Trenary [33] reported that the variability of the $\delta_s(CH_3)$ mode in surface infrared spectra is actually a general feature of CH_3Y (Y = I, Br, Cl, F, C_6H_5, etc.) molecules where the infrared intensity of the $\delta_s(CH_3)$ mode varies strongly with the nature of the substituent group, Y. There is a correlation between the intensity of $\delta_s(CH_3)$ and ν_s(C–H) and the polarization of CH_3^+–Y^- due to the inductive effect of the substituent. The $\delta_s(CH_3)$ band is weak when the polarization is either weak or strong, but ν_s(C–H) is strong only when the polarization of CH_3^+–Y^- is weak. Assuming that this effect also occurs with CH_2 groups, our results would suggest that the carbon–silver bond of CH_2 is covalent-like with a weak polarization between silver and methyl. The lack of the deformation bands of CH_2(a) in our case could also indicate total dipole screening caused by the strongly ionic I-covered surface.

By 240 K, no trace of CH_2(a) remains in RAIRS. TPD indicates that CH_2 groups leave the surface as C_2H_4, and the absence of RAIRS signal from C_2H_4 indicates that C_2H_4 desorbs from the surface in a reaction-limited process. This behavior is in agreement with previous TPD results, as C_2H_4 desorption from Ag(111) occurs below 150 K [34] and C_2H_4 desorption from Ag(111) pre-covered with I occurs at 115 K, as shown in figure 2(A).

4.2. *Thermally activated reactions of CH_2I_2 on Ag(111) pre-covered with O*

The effect of O(a) is twofold. Pre-adsorbed O not only limits the formation of C_2H_4 as a blocking agent, but it is also a reaction partner that consumes CH_2 groups. CH_2I_2 is strongly stabilized by O(a), indicated by the presence of the characteristic vibration modes of CH_2I_2 well above 200 K, as shown in figure 6. At 0.1 ML O(a) coverage, the stabilization by O(a) is weaker (not shown) when compared to 0.5 ML O(a) as indicated by the disappearance of the CH_2I_2 vibrational bands by 220 K. The $\nu_a(CH_2)$ mode at 3060 cm^{-1} on the O-saturated surface is still visible after annealing to 260 K, where on the clean surface the $\nu_a(CH_2)$ mode at 3044 cm^{-1} disappears after annealing to 200 K. At 80 K the characteristic peaks of CH_2I_2 are located at higher vibrational frequency (3057, 2974, and 1114 cm^{-1}) than on the clean surface (3044, 2968, and 1110 cm^{-1}). As the annealing temperature increases the $\nu_a(CH_2)$ and $\nu_s(CH_2)$ bands blue shift slightly to 3060 and 2979 cm^{-1}, respectively, indicating a more pronounced interaction between adsorbed O and CH_2I_2. Two of the vibrational bands,

$\delta(CH_2)$ and $\rho(CH_2)$, that are clearly visible on clean Ag(111) are not present on Ag(111) pre-covered with O.

The desorption features of the parent CH_2I_2 molecule do not change when Ag(111) is pre-covered with O(a) when compared to the clean surface; the intact CH_2I_2 molecules desorb only from the condensed layer. The CH_2I_2 species bonded in the chemisorbed state decompose via C–I bond cleavage, thus the stabilization effect of O(a) is not reflected in the parent desorption feature as it is on Rh(111) [11,13] and Ru(001) [15]. Interestingly, pre-adsorbed O, even at its saturation coverage, does not increase the amount of the desorbed CH_2I_2 as opposed to pre-adsorbed I, which is an effective site blocker and thus dramatically increases the amount of desorbed CH_2I_2. Presumably, this effect is due to the large difference between the van der Waals radii of O and I (1.40 and 2.15 Å for O and I, respectively).

In contrast, the presence of O(a) is more pronounced in hindering the coupling of CH_2(a) groups when compared to I(a), as shown in figure 5. For clean Ag(111) we postulate that the high-temperature C_2H_4 desorption feature at 230 K is due to increased site blocking during the temperature ramp of the experiment due to decomposition of CH_2I_2. We speculate that the reduction in the amount of C_2H_4 in the case of Ag(111) pre-adsorbed with O originates not only from site blocking but also from a reaction consuming CH_2 groups.

A surface reaction is thought to occur between the O(a) and adsorbed CH_2-containing species. The increased interaction between O(a) and CH_2I_2(a) is indicated by the blue shift of the CH_2I_2 infrared bands, as seen in figure 6. The lack of infrared vibrations characteristic of CH_2(a) in figure 6 suggests that either there is no thermal C–I bond breaking to produce CH_2(a) groups or CH_2(a) groups immediately react to form another species. Because of the lack of the infrared bands we suspect that the reaction that consumes CH_2 groups takes place mainly between adsorbed CH_2I_2 and O in an S_{N2}-like manner. However, the possibility of direct reaction of CH_2(a) and O(a) should also be considered on the basis of the reaction of CH_2 and O on other surfaces [9–11,14,15]. The main product of this substitution reaction is CH_2O. Presumably, the partial negative charge of the O(a) and the partial positive charge located on C interact, thus explaining the stabilization effect of O(a) on the CH_2I_2 molecules and the formation of CH_2O. Above 0.1 ML O(a) coverage a high-temperature peak appears on the CH_2O desorption feature in figure 4, which increases with increasing O coverage. The CH_2O desorption spectrum on Ag(111) pre-adsorbed with O can be fitted to two peaks centered at 228 and 267 K. The two desorption features are related to the presence of two different O(a) phases on the surface as suggested earlier.

For up to 0.1 ML doses of O(a), the chemisorbed O reacts, while at saturation mainly the more ionic oxide phase does [18,21]. The ionic O(a) carrying larger negative charge contributes to the enhanced amount of CH_2O formation with a peak temperature of 267–270 K. CH_2O cannot be detected on the surface using RAIRS because the desorption temperature of CH_2O is below 120 K [35], clearly indicating a reaction-limited process above 200 K. The upward shift in the CH_2O desorption temperature, going from the chemisorbed to the oxide-like phase, indicates that besides the nucleophilic attack of the negative charged O(a), bond strength also plays an important role in the formation temperature of CH_2O. In other words, with respect to the co-adsorbed CH_2I_2 molecules, O in the oxide phase is more stable than O in the chemisorbed state.

Another reaction product is detectable in both TPD and RAIRS suggesting that there is another reaction path affecting the product distribution. CH_2I_2 molecules or, more probably, CH_2(a) make chemical contact with two O atoms on the surface resulting in formate, HCOO. In figure 6 a very faint band at 2810 cm^{-1} in the 260 K spectrum is assigned to the Fermi resonance of ν(CH) with 2δ(CH) or ν_a(OCO) + δ(CH) for the formate species. This species should have a strong deformation band near 1320 cm^{-1} [36], but in our case I(a) affects the vibrational extinction coefficients of the adsorbed species, as noted earlier with the vibration characteristics of CH_2(a) on I-covered Ag(111). The formation of formate can occur not only at the saturation O(a) coverage, but at any coverage above 0.05 ML O because p(4 × 4)–O islands can form locally under our experimental conditions [18,21].

The formation of HCOO represents a minor reaction route. Increasing the surface coverage of O(a) increases the extent of oxidation and the production of both CH_2O and HCOO. Even though the amount of HCOO increases more rapidly than CH_2O, its concentration is below 1% of the total products, thus explaining the small intensity of the infrared band characteristic of HCOO.

Above 260 K there are no visible vibrations, but the desorption of CO_2 can be observed until ~400 K, as seen in figure 4. HCOO decomposes to CO_2 and H_2 as on other transition metal surfaces [37]. CO_2 desorption was detected with a peak temperature from 340 to 355 K. The amount of CO_2 increases with increasing formation of HCOO but, as noted above, its concentration is very low. Unfortunately, our TPD experiments were not sensitive to H_2 and thus we were not able to detect H_2 desorption. Above 400 K the only species remaining on the surface are I(a) and a reduced amount of O, which desorb at 820–850 and 560 K, respectively. The suggested reaction scheme summarizing our experimental results for the decomposition of CH_2I_2 in the presence of O(a) and the formation of O-containing species is shown in figure 7.

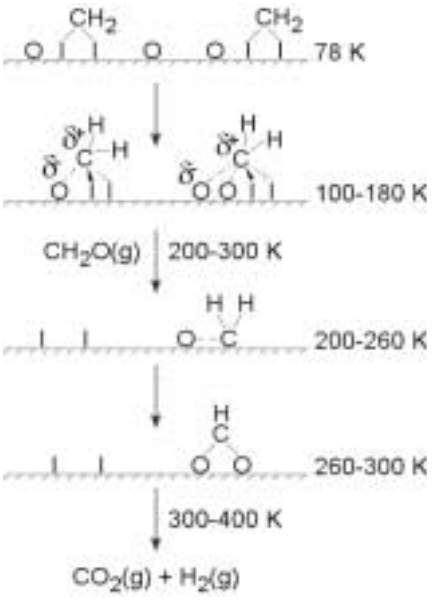

Figure 7. Reaction scheme for the decomposition of CH_2I_2 adsorbed on O-modified Ag(111).

5. Conclusions

We have shown that CH_2I_2 adsorbs dissociatively at low coverages at 78 K to form CH_2(a) and I(a). CH_2(a) groups react to form C_2H_4(g) that desorbs in a reaction-limited process during the TPD temperature ramp. As the coverage of CH_2I_2 is increased on the clean surface, the dissociation of the CH_2I_2 groups is hindered by the crowding on the surface, causing the C_2H_4 desorption feature to shift to higher temperatures.

When CH_2I_2 is dosed onto Ag(111) pre-adsorbed with O(a), CH_2O forms as a major reaction product. Two different states of CH_2O are distinguished according to the presence of O atoms in chemisorbed and oxide-like phase. CH_2O is suggested to form from CH_2I_2, stabilized by the surface O. O(a) also acts as a site blocker to reduce C_2H_4 formation. There is a minor secondary reaction route, the formation of formate, which is indicated by the desorption of CO_2 groups and a vibrational band in the RAIR spectra at 2810 cm^{-1}. The formation of formate is not sensitive to the character of O(a), but reaction yield increases with increasing O coverage.

Acknowledgements

This work is supported by the National Science Foundation and the Hungarian Academy of Sciences, Grants CHE 0070122, INT 9722819 and OTKA Grant T032040. J.M.W. acknowledges the support of the Robert A. Welch Foundation. The authors would like to thank Dr. Chulhoon Kim for assistance with TOF-TPD experiments, Dr. Hugo Celio for fruitful discussions, and Tim Rountree for aid in crystal polishing.

References

[1] D.M. Bibby, C.D. Chang, R.F. Howe and S. Yurchak, in: *Studies in Surface Science and Catalysis*, *Symposium on the Production of Fuels and Chemicals from Natural Gas*, eds. B. Delmon and J.J.T. Yates (Auckland, Elsevier, 1988) p. 741.
[2] F. Solymosi, in: *Molecular Chemistry of Alkane Activation*, ed. E.G. Derouane (Kluwer Academic, Dordrecht, 1998).
[3] X.L. Zhou and J.M. White, J. Phys. Chem. 95 (1991) 5575.
[4] X.L. Zhou, F. Solymosi, P.M. Blass, K.C. Cannon and J.M. White, Surf. Sci. 219 (1989) 294.
[5] X.L. Zhou, M.E. Castro and J.M. White, Surf. Sci. 238 (1990) 215.
[6]. B.E. Bent, Chem. Rev. (Washington, D.C.) 96 (1996) 1361, and references therein.
[7] G.C. Bond, *Catalysis by Metals* (Academic Press, New York, 1962).
[8] X.L. Zhou, X.Y. Zhu and J.M. White, Surf. Sci. Rep. 13 (1991) 73.
[9] X.L. Zhou, Z.M. Liu, J. Kiss, D.W. Sloan and J.M. White, J. Am. Chem. Soc. 117 (1995) 3565.
[10] F. Solymosi, I. Kovacs and K. Revesz, Surf. Sci. 356 (1996) 121.
[11] F. Solymosi and G. Klivenyi, J. Phys. Chem. 99 (1995) 8950.
[12] C.W.J. Bol and C.M. Friend, Surf. Sci. 337 (1995) L800.
[13] C.W.J. Bol and C.M. Friend, J. Am. Chem. Soc. 117 (1995) 11572.
[14] I. Kovacs and F. Solymosi, J. Mol. Catal. A 141 (1999) 31.
[15] A. Kis, J. Kiss and F. Solymosi, Surf. Sci. 459 (2000) 149.
[16] R.A. Van Santen and H.P.C.E. Kuipers, Adv. Catal. 35 (1987) 265.
[17] T. Schedel-Niedrig, X. Bao, M. Muhler and R. Schlogl, Ber. Bunsen-Ges. 101 (1997) 994.
[18] V.I. Bukhtiyarov, V.V. Kaichev and I.P. Prosvirin, J. Chem. Phys. 111 (1999) 2169.
[19] C.T. Campbell, Surf. Sci. 157 (1985) 43.
[20] C.I. Carlisle, D.A. King, M.L. Bocquet, J. Cerda and P. Sautet, Phys. Rev. Lett. 84 (2000) 3899.
[21] C.I. Carlisle, T. Fujimoto, W.S. Sim and D.A. King, Surf. Sci. 470 (2000) 15.
[22] W.S. Sim, P. Gardner and D.A. King, J. Phys. Chem. 99 (1995) 16002.
[23] S.R. Bare, K. Griffiths, W.N. Lennard and H.T. Tang, Surf. Sci. 342 (1995) 185.
[24] G. Polzonetti, P. Alnot and C.R. Brundle, Surf. Sci. 238 (1990) 237.
[25] G. Polzonetti, P. Alnot and C.R. Brundle, Surf. Sci. 238 (1990) 226.
[26] G. Rovida, F. Pratesi, M. Maglietta and E. Ferroni, Surface Sci. 43 (1974) 230.
[27] B.H. Torrie, A. Anderson, B. Andrews, D.G. Laurin, J.K. White and W.W.E. Zung, J. Raman Spectrosc. 18 (1987) 215.
[28] J.N. Kondo, T. Higashi, H. Yamamoto, M. Hara, K. Domen and T. Onishi, Surf. Sci. 349 (1996) 294.
[29] T. Livneh and M. Asscher, Langmuir 14 (1998) 1348.
[30] M.K. Weldon and C.M. Friend, Surf. Sci. 321 (1994) L202.
[31] J. Kiss, R. Barthos and F. Solymosi, Top. Catal. 14 (2001) 145.
[32] P.M. George, N.R. Avery, W.H. Weinberg and F.N. Tebbe, J. Am. Chem. Soc. 105 (1983) 1393.
[33] J. Fan and M. Trenary, Langmuir 10 (1994) 3649.
[34] K. Kershen, H. Celio, I. Lee and J.M. White, Langmuir 17 (2001) 323.
[35] L.E. Fleck, Z.C. Ying, M. Feehery and H.L. Dai, Surf. Sci. 296 (1993) 400.
[36] W.S. Sim, P. Gardner and D.A. King, J. Phys. Chem. 100 (1996) 12509.
[37] D.H.S. Ying and R.J. Madix, J. Catal. 61 (1980) 48.
[38] M.P. Marzocchi, V. Schettino and S. Califano, J. Chem. Phys. 45 (1966) 1400.